

# Expert Knowledge-driven Reinforcement Learning for Autonomous Racing via Trajectory Guidance and Dynamics Constraints

Bo Leng<sup>a</sup>, Weiqi Zhang<sup>a</sup>, Zhuoren Li<sup>a,\*</sup>, Lu Xiong<sup>a</sup>, Guizhe Jin<sup>a</sup>, Ran Yu<sup>a</sup> and Chen Lv<sup>b</sup>

<sup>a</sup>College of Automotive and Energy Engineering, Tongji University, Shanghai, 201804, China

<sup>b</sup>School of Mechanical and Aerospace Engineering, Nanyang Technological University, Singapore, 639798, Singapore

## ARTICLE INFO

### Keywords:

Autonomous Racing  
Reinforcement Learning  
Racing Line Guidance  
Dynamics Constraints  
Curriculum Learning

## ABSTRACT

Reinforcement learning has demonstrated significant potential in the field of autonomous driving. However, it suffers from defects such as training instability and unsafe action outputs when faced with autonomous racing environments characterized by high dynamics and strong nonlinearities. To this end, this paper proposes a trajectory guidance and dynamics constraints Reinforcement Learning (TraD-RL) method for autonomous racing. The key features of this method are as follows: 1) leveraging the prior expert racing line to construct an augmented state representation and facilitate reward shaping, thereby integrating domain knowledge to stabilize early-stage policy learning; 2) embedding explicit vehicle dynamic priors into a safe operating envelope formulated via control barrier functions to enable safety-constrained learning; and 3) adopting a multi-stage curriculum learning strategy that shifts from expert-guided learning to autonomous exploration, allowing the learned policy to surpass expert-level performance. The proposed method is evaluated in a high-fidelity simulation environment modeled after the Tempelhof Airport Street Circuit. Experimental results demonstrate that TraD-RL effectively improves both lap speed and driving stability of the autonomous racing vehicle, achieving a synergistic optimization of racing performance and safety.

## 1. Introduction

Autonomous racing has emerged as an important sub-field of autonomous driving research. It features highly dynamic manoeuvres, strongly nonlinear vehicle behavior, and operating near the physical limits of handling. The primary objective is to minimize lap time while complying with race regulations and safety constraints. Autonomous race cars operate at high speeds and large accelerations, often with very little margin for error. This makes racing a demanding benchmark for decision-making and control methods that must remain reliable near the limits of feasibility. Moreover, it is also a quintessential safety-critical domain. Progress in this area drives decision-making and control methods that balance performance with safety and are suitable for verification and deployment. Recently, a growing body of work has examined planning, decision-making and control, and competitive interaction in autonomous racing [1–3]. International competitions such as the Indy Autonomous Challenge (IAC) [4, 5] and the Abu Dhabi Autonomous Racing League (A2RL) [6, 7] have also attracted sustained participation from academia and industry, helping to drive rapid advances and keeping the field highly active.

Although traditional methods, such as Model Predictive Control (MPC) [8], have shown promising results in autonomous racing tasks, they still face limitations in terms of model accuracy, real-time performance and robustness [9]. These methods typically divide the autonomous racing system into two modules: path planning and trajectory tracking. The planner generates an optimal trajectory based on

vehicle and track information, while the controller follows that trajectory. However, in high-speed conditions, tires are often pushed to the friction limit, leading to highly nonlinear behavior [10]. Consequently, traditional optimization-based and rule-driven control strategies often struggle in these highly dynamic environments. Their rigid reliance on explicit mathematical formulations and predefined heuristics restricts the vehicle from fully exploiting its physical limits, leading to overly conservative driving behaviors and poor adaptability to unmodeled disturbances [11].

As learning-based methods have demonstrated significant potential in high-dynamics control tasks [12, 13], researchers have started to explore the use of learning-based decision-making and control in autonomous racing. This reduces reliance on precise modeling and enhances adaptability to strong nonlinearity and uncertainty. A representative approach is the incorporation of learning mechanisms into traditional MPC frameworks, leading to Learning-based MPC (LMPC). For example, [14] proposed a data-driven MPC controller based on online learning that uses Gaussian process regression to model residual uncertainties, allowing safer driving behaviors. [15] applied local linear, data-driven dynamic error learning to compensate for a nominal global nonlinear physical model, improving prediction accuracy and control performance under extreme operating conditions. Meanwhile, some studies have adopted imitation learning (IL) to learn racing strategies from expert or human demonstrations. For example, [16] utilized human player demonstrations combined with adversarial imitation learning to improve the strategy's adaptability to new environments and distribution shifts. Despite the progress made by these learning-based methods in autonomous racing, LMPC

\*Corresponding author: Zhuoren Li (1911055@tongji.edu.cn)

✉ lengbo@tongji.edu.cn (B. Leng); 2511517@tongji.edu.cn (W. Zhang)

Zhang)

ORCID(s):

still faces challenges related to model adaptation and parameter uncertainty, while imitation learning relies on high-quality expert demonstration datasets, which are difficult to obtain in practical applications.

Reinforcement Learning (RL) methods are more widely used in autonomous racing. By training agents through experience, the RL agent optimizes strategies based on reward feedback [17]. RL does not require explicit model descriptions, making it particularly suited for tasks with high-dimensional state spaces and complex decision-making [18]. The core advantage of RL lies in maximizing long-term rewards, which aligns well with the goal of continuously optimizing lap times in racing tasks. RL has demonstrated performance that matches or exceeds human racers on various simulation platforms and even some physical systems [19, 20]. For instance, Fuch et al. [19] utilized a course-progress proxy reward in Gran Turismo Sport, achieving lap times faster than both the in-game AI and over 50,000 human players. Wurman et al. [20] proposed a deep reinforcement learning approach that enabled an agent to outperform champion drivers in Gran Turismo Sport, showcasing RL's potential in high-performance autonomous racing tasks.

However, traditional RL methods typically require extensive interaction with the environment to optimize through trial and error, which results in low sample efficiency, high costs, and difficulty in iterative training in dynamic physical systems [21]. Additionally, in tasks with sparse rewards or narrow feasible regions, the lack of structured exploration guidance makes it challenging to obtain meaningful reward signals. This can result in slow convergence, unstable training, and the risk of ineffective exploration [22]. More importantly, standard RL methods often neglect explicit modeling of safety constraints, failing to ensure their strict satisfaction. As a result, trial-and-error exploration during training may produce unsafe actions and violate constraints [23]. If relying solely on safety rewards often fails to ensure the strict satisfaction of constraints, leading to unstable policy behavior and increasing unforeseen risks during deployment.

To address the aforementioned challenges, this paper proposes a **T**rajectory guidance and **D**ynamics constraints **R**einforcement **L**earning (TraD-RL) decision-making and control framework for autonomous racing. Specifically, expert prior knowledge, encompassing trajectory guidance and dynamics constraints, is explicitly embedded within the training process. The overall framework is illustrated in Fig. 1. First, to tackle the issues of low exploration efficiency and the difficulty of learning optimal trajectories in complex racing environments, we encode track geometric priors and racing intent into structured guidance information using the racing line. This approach enhances the learning efficiency and stability of the agent within high-dimensional spaces. Second, to reduce the risk of instability inherent in high-speed racing, we explicitly introduce vehicle dynamics stability constraints during policy learning. By comprehensively considering two key stability indicators, yaw rate and sideslip angle, this mechanism effectively suppresses unsafe behaviors and enhance deployability. Finally, to fully exploit

the racing potential while ensuring training convergence, we develop a two-stage curriculum learning strategy based on dynamic task evolution. This facilitates a smooth transition of the model's capabilities toward limit-handling dynamic racing. The main contributions of this paper are as follows:

- 1) We propose a reinforcement learning state representation and reward shaping mechanism guided by global trajectory priors. By leveraging global track geometry, the Minimum Curvature Racing Line (MCRL) is pre-calculated to serve as a global optimal reference. We then construct a reference-augmented observation space to explicitly embed this high-value geometric prior information into the policy network. Building on this, we design a hybrid dense reward function that incorporates constraints on tracking position, target speed, and heading alignment. This mechanism effectively confines the agent's exploration scope to the vicinity of the optimal trajectory, thereby addressing the sparse reward challenge inherent in high-dimensional continuous action spaces. Consequently, it enables the autonomous racing vehicle to rapidly converge to an expert-level driving policy that balances both speed and stability;
- 2) We introduce a policy regularization method based on explicit dynamics constraints prior. By imposing constraints on the yaw rate and vehicle sideslip angle, we characterize the safe operating envelope within the sideslip angle-yaw rate phase plane to serve as a control prior. This prior is formalized as a differentiable constraint term  $h(x)$  via Control Barrier Functions (CBFs) and is embedded into the policy optimization objective using Lagrangian Relaxation. By employing two learnable adaptive Lagrangian multipliers, the system dynamically regulates its adherence to the control prior. This mechanism imposes physics-informed soft constraints during trial-and-error exploration, effectively suppressing instability while maintaining exploration viability;
- 3) We propose a progressive two-stage curriculum learning strategy. This strategy partitions the learning process into a trajectory guidance stage and a high-speed exploration stage. In the trajectory guidance stage, a target speed tracking reward is utilized to guide the racing car to drive stably at the reference speed. Subsequently, the high-speed phase adopts a maximum-velocity reward, encouraging the agent to approach the vehicle's physical limits at the highest possible speed. By implementing an 'easy-to-hard' training schedule through this progressive reward formulation, we significantly enhance both the learning efficiency and the racing performance of the reinforcement learning agent.

The remainder of the paper is organized as follows: In section 2, some preliminaries are introduced and the racing problem is defined. The methodology is elaborated in Section 3. In Section 4, simulation testing and discussion of proposed method are presented. Finally, Section 5 concludes this work.

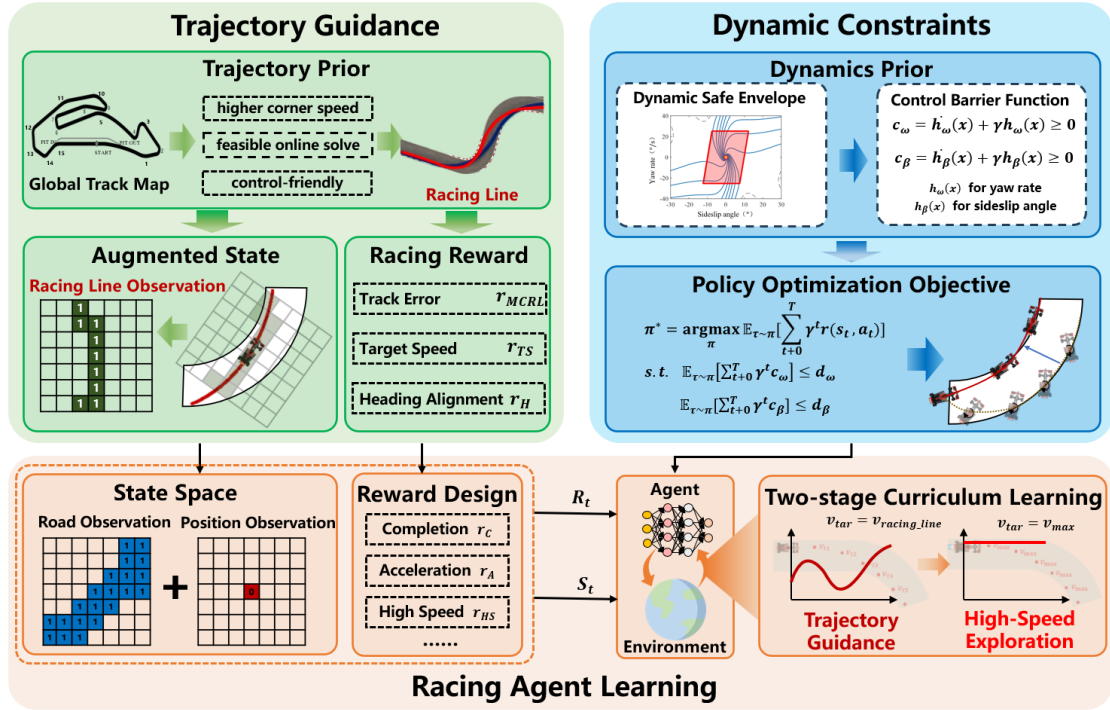


Figure 1: The reinforcement learning decision-making and control framework driven by expert prior knowledge..

## 2. Preliminaries

### 2.1. Reinforcement Learning

Reinforcement learning is typically mathematically formalized as a Markov Decision Process (MDP), defined by the tuple  $\mathcal{M} = \langle \mathcal{O}, \mathcal{A}, \mathcal{P}, \mathcal{R}, \gamma \rangle$ . Here,  $\mathcal{O}$  denotes the state space,  $\mathcal{A}$  represents the action space,  $\mathcal{P} : \mathcal{O} \times \mathcal{A} \times \mathcal{O} \rightarrow [0, 1]$  is the state transition probability function,  $\mathcal{R} : \mathcal{O} \times \mathcal{A} \rightarrow \mathbb{R}$  is the reward function, and  $\gamma \in [0, 1)$  serves as the discount factor. At each discrete time step  $t$ , the agent observes the current state  $o_t \in \mathcal{O}$  and selects an action  $a_t \in \mathcal{A}$  according to a policy network  $\pi_\theta(a_t|o_t)$ , parameterized by  $\theta$ . The policy is typically constructed using neural networks (NNs) with the aim of fitting arbitrarily complex policy distribution functions. The primary objective of the agent is to determine an optimal policy  $\pi_\theta^*$  that maximizes the expected cumulative discounted return  $J(\pi_\theta)$ :

$$J(\pi_\theta) = \mathbb{E}_{\tau \sim \pi_\theta} \left[ \sum_{t=0}^{\infty} \gamma^t r(o_t, a_t) \right] \quad (1)$$

where  $\tau = (o_0, a_0, o_1, a_1, \dots)$  denotes the trajectory of state-action pairs.

To evaluate the performance of a policy, we define the state-value function  $V^\pi(o)$  and the action-value function  $Q^\pi(o, a)$ . These functions satisfy the following Bellman expectation equations:

$$V^\pi(o_t) = \mathbb{E}_{a_t \sim \pi, o_{t+1} \sim \mathcal{P}} [r(o_t, a_t) + \gamma V^\pi(o_{t+1})] \quad (2)$$

$$Q^\pi(o_t, a_t) = \mathbb{E}_{o_{t+1} \sim \mathcal{P}, a_{t+1} \sim \pi} [r(o_t, a_t) + \gamma Q^\pi(o_{t+1}, a_{t+1})] \quad (3)$$

where  $V^\pi(o_t)$  measures the long-term value of being in a specific state, while  $Q^\pi(o_t, a_t)$  evaluates the value of taking a specific action from that state. Together, these equations serve as the theoretical foundation for value estimation and policy gradient computation.

In summary, the objective  $J(\pi_\theta)$  provides the optimization goal for the agent, while the state-value and action-value functions serve as the essential metrics for evaluating the performance of the current policy  $\pi_\theta$ . The Bellman expectation equations establish the recursive consistency required to compute these value functions accurately. By solving these equations, the agent can effectively map its long-term objective into a series of local updates, enabling the improvement of the policy towards the global optimum  $\pi_\theta^*$ .

### 2.2. Vehicle Dynamics

We employ a Dynamic Bicycle Model to capture lateral and yaw motion characteristics while maintaining computational efficiency. As illustrated in Fig. 2, the vehicle is simplified as a single-mass rigid body on a two-dimensional plane. The state vector is defined as  $X = [x, y, \varphi, u, v, \omega]^T$ , where  $(x, y)$  denotes the inertial position,  $\varphi$  is the heading angle,  $u$  and  $v$  represent the longitudinal and lateral velocities in the body frame, and  $\omega$  is the yaw rate.

Adopting the Small Angle Approximation, the differential equations governing the vehicle dynamics are expressed as:

$$\begin{aligned} m(\dot{v} + u\omega) &= F_{yf} \cos \delta + F_{yr} \\ I_z \dot{\omega} &= l_f F_{yf} \cos \delta - l_r F_{yr} \end{aligned} \quad (4)$$

where  $m$  denotes the total vehicle mass,  $I_z$  represents the yaw moment of inertia about the  $z$ -axis, and  $l_f$  and  $l_r$  are

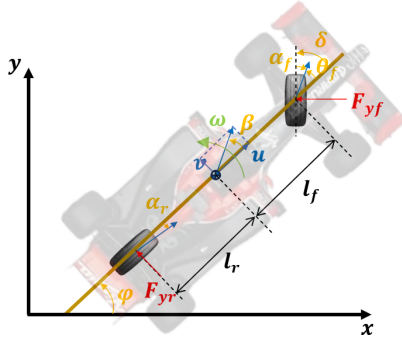


Figure 2: Vehicle Dynamics Model.

the distances from the center of mass to the front and rear axles, respectively.

From the differential equations, the system state-space representation,  $\dot{X} = f(X, U)$ , is derived as follows:

$$\dot{X} = f(X, U) = \begin{bmatrix} u \cos \varphi - v \sin \varphi \\ u \sin \varphi + v \cos \varphi \\ \omega \\ a + v\omega - \frac{1}{m}F_{yf} \sin \delta \\ -u\omega + \frac{1}{m}(F_{yf} \cos \delta + F_{yr}) \\ \frac{1}{I_z}(l_f F_{yf} \cos \delta - l_r F_{yr}) \end{bmatrix} \quad (5)$$

where  $U = [a, \delta]^T$  is the control input,  $a$  and  $\delta$  represent longitudinal acceleration and the front-wheel steering angle, respectively.

To ensure both the efficiency and fidelity of the vehicle dynamic response, the interaction between the tires and the road is modeled within the linear elastic range. The lateral tire forces at the front and rear axles,  $F_{yf}$  and  $F_{yr}$ , are proportional to their respective slip angles,  $\alpha_f$  and  $\alpha_r$ , i.e.,  $F_{yf} = C_{\alpha_f} \alpha_f$ ,  $F_{yr} = C_{\alpha_r} \alpha_r$ , where  $C_{\alpha_f}$  and  $C_{\alpha_r}$  denote the cornering stiffness of the front and rear tires, respectively. Based on the kinematic relationships, the slip angles are defined as:

$$\begin{aligned} \alpha_f &= \delta - \arctan\left(\frac{v + l_f \omega}{u}\right) \\ \alpha_r &= -\arctan\left(\frac{v - l_r \omega}{u}\right) \end{aligned} \quad (6)$$

### 3. Methodology

The autonomous racing task is defined as a constrained time-optimal control problem and is formulated as MDP. The goal is to minimize lap time subject to strict vehicle dynamics and geometric track constraints. Within this formulation, a reinforcement learning agent learns to map local observations to continuous control inputs, specifically longitudinal acceleration and steering angle. This approach enables the derivation of a precise and safety-constrained policy through sequential interaction with the environment.

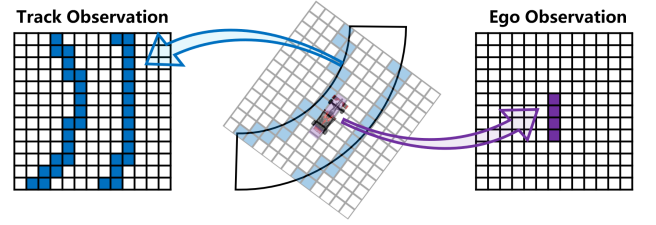


Figure 3: Schematic diagram of the ego-centric grid observation space construction.

### 3.1. RL Racing Framework

**Observation Space** This paper adopts an ego-centric occupancy grid map as the fundamental representation of the observation space in order to describe the unstructured road features of the racetrack.

The observation vector consists of two parts: environmental geometric features and vehicle kinematic states, as illustrated in Fig. 3. Specifically, the environmental features primarily consist of the track boundary observation  $o_{\text{track}}$ . The vehicle state observation includes the ego-vehicle's lateral velocity  $o_{\text{ego}_v}$ , longitudinal velocity  $o_{\text{ego}_u}$ , and heading angle  $o_{\text{ego}_h}$ .

Regarding the feature encoding strategy, we employ a spatially aligned numerical mapping method: For track observation, binary encoding is used. Grid cells containing track boundary points take the value 1, while the others are 0. For ego-vehicle observation, numerical embedding encoding is used. The kinematic states of the ego-vehicle are inserted into the grid cells occupied by its geometric center. Furthermore, if expert prior knowledge is incorporated, the observation space will include the trajectory guidance information  $o_{\text{MCRL}}$ . The details are presented in 3.2.2.

**Action Space** This paper constructs a continuous and decoupled two-dimensional action space. Specifically, at each time step, the reinforcement learning agent directly outputs the longitudinal acceleration command  $a$  and the front-wheel steering angle command  $\delta$ . Furthermore, to enhance the convergence rate and numerical stability of the network training, all output actions are normalized to the interval  $[-1, 1]$ .

**Reward Function Design** To encourage the agent to complete the racing task as quickly as possible, this paper designs a multi-dimensional basic reward function. This function primarily consists of four components: the track constraint reward, velocity performance reward, acceleration smoothness reward, and progress completion reward.

**Track Constraint Reward:** To ensure the race car operates within the drivable area, we define a track constraint reward:

$$r_{\text{track}} = \begin{cases} 1 & \text{on track} \\ -2 & \text{off track} \end{cases} \quad (7)$$

**High-Speed Reward:** When the speed falls within the high-speed range  $[u_{h1}, u_{h2}]$ , the reward increases linearly with speed.

$$r_{hs} = \frac{u - u_{h1}}{u_{h2} - u_{h1}} \quad (8)$$

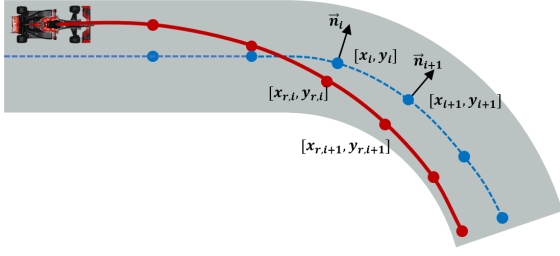


**Figure 4:** Parameterization of the optimal racing line relative to the track centerline.

**Low-Speed Reward:** When the speed falls within the low-speed range  $[u_{l1}, u_{l2}]$ , a penalty inversely proportional to speed is applied.

$$r_{ls} = 1 - \frac{u}{u_{l2}^2} \quad (9)$$

**Lap Completion Reward:** To incentivize the agent to successfully complete a full lap, a discrete terminal reward  $r_{lap}$  is granted whenever the vehicle crosses the finish line.

$$r_{lap} = \begin{cases} 1, & \text{if a full lap is completed} \\ 0, & \text{otherwise} \end{cases} \quad (10)$$

Finally, to eliminate magnitude discrepancies among different rewards and enhance numerical stability, all rewards designed in this paper are normalized to the interval  $[-1, 1]$ .

### 3.2. Trajectory Prior Guidance

In the context of high-speed, highly dynamic autonomous racing, reinforcement learning often suffers from inefficient exploration due to the continuous action space and sparse environmental rewards. To address these challenges, this paper proposes a Trajectory Prior Guidance method, aimed at bridging the gap between random exploration and optimal control by incorporating expert knowledge. This expert trajectory is utilized not only to construct dense reward functions but also directly for observation space augmentation. This approach narrows the search range of the policy, thereby enhancing the training stability and convergence speed of the algorithm.

#### 3.2.1. Racing Line Generation

The geometric features of the track can be characterized by a reference line. This line consists of a series of discrete global coordinates  $[x_i, y_i]^T$ , and includes the distance information to the left and right track boundaries for each point, denoted as  $w_{left,i}$  and  $w_{right,i}$ , respectively. To generate the optimal racing line, we formulate the path planning task as a lateral offset optimization problem relative to the reference line, as illustrated in Fig. 4. Specifically, the  $i$ -th waypoint on the racing line  $[x_{r,i}, y_{r,i}]^T$  is obtained by applying a lateral displacement along the normal vector  $\vec{n}_i$  of the corresponding reference point:

$$[x_{r,i}, y_{r,i}]^T = [x_i, y_i]^T + \sigma_i \vec{n}_i \quad (11)$$

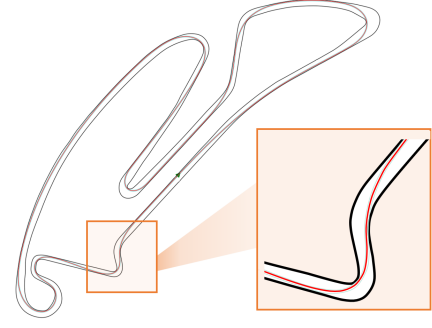


**Figure 5:** Illustration of MCRL. The black lines indicate track boundaries, the red line shows the generated MCRL trajectory, and the cyan lines represent vehicle boundaries.

where  $\sigma_i$  is the scalar parameter to be optimized, determining the lateral displacement distance of the racing line waypoint along the normal direction. To ensure the racing line always remains within the drivable area and avoids collisions, the value range of  $\sigma_i$  is jointly determined by the track geometry and the vehicle width  $w_{veh}$ :

$$\sigma_i \in \left[ -w_{left,i} + \frac{w_{veh}}{2}, w_{right,i} - \frac{w_{veh}}{2} \right] \quad (12)$$

This paper defines the optimization objective as the minimization of the sum of squared curvatures along the discrete path:

$$\begin{aligned} \min_{\sigma_1, \dots, \sigma_N} \quad & \sum_{i=1}^N \kappa_i^2(t) \\ \text{s.t.} \quad & \sigma_i \in \left[ -w_{left,i} + \frac{w_{veh}}{2}, w_{right,i} - \frac{w_{veh}}{2} \right] \end{aligned} \quad (13)$$

An iterative optimization strategy is employed considering the non-linearity of curvature calculation and potential errors introduced by single-step linearization [24]. By iteratively refining the curvature until the difference between two adjacent iterations converges within a preset threshold  $\varepsilon$  ( $|\kappa_{n+1} - \kappa_n| \leq \varepsilon$ ), the racing line achieves higher geometric accuracy. Meanwhile, this process effectively eliminates local curvature peaks, yielding a trajectory that better aligns with the vehicle's kinematic characteristics. The Minimum Curvature Racing Line (MCRL) is illustrated in Fig. 5.

Subsequently, based on the vehicle's GGV performance envelope, we generate a reference velocity profile using a forward-backward integration strategy. Finally, the generated expert prior trajectory is encapsulated into a six-dimensional state vector  $[s, x, y, \varphi, \kappa, u]$ , comprising curvilinear distance  $s$ , inertial coordinates  $(x, y)$ , heading angle  $\varphi$ , curvature  $\kappa$ , and longitudinal velocity  $u$ .

#### 3.2.2. Observation Augmentation

Based on the racing line data generated above, we augment the primary observation space by constructing the racing line observation feature  $o_{MCRL}$ . As illustrated in Fig. 6, this feature is constructed within the ego-centric local coordinate system and encoded using a binary occupancy

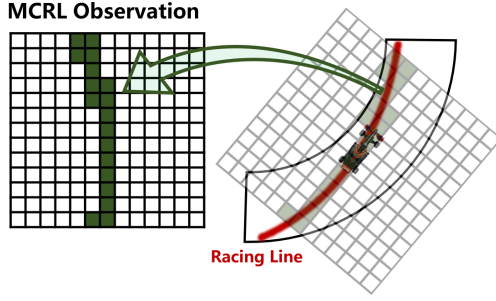


**Figure 6:** Schematic illustration of mapping the racing line prior into the occupancy grid.

grid. Specifically, grid cells covering the racing line waypoints take the value 1, while the remaining areas are 0. The incorporation of this expert prior information significantly enhances training efficiency. It not only assists the agent in rapidly comprehending the trajectory guidance mechanism but also effectively compresses the policy exploration space, enabling precise acquisition of the driving policy.

### 3.2.3. Reward Shaping

In order to utilize expert prior knowledge to guide the agent's policy optimization process, the reward function is further refined through reward shaping. Specifically, three core reward components are constructed based on trajectory tracking error, speed tracking error, and heading alignment relative to the MCRL.

- **Trajectory Tracking Reward:** This reward aims to guide the race car to strictly adhere to the optimal trajectory coordinates. Let  $l$  denote the Euclidean distance between the vehicle's current position  $[x, y]^T$  and the nearest reference point  $[x_r, y_r]^T$  on the racing line.

$$r_{\text{MCRL}} = \frac{1}{1 + l^2} \quad (14)$$

- **Target Speed Tracking Reward:** We set the target speed  $u_{tar}$  to the reference speed at the look-ahead point using a preview mechanism. This reward guides the agent to acquire the optimal longitudinal speed control strategy adapted to different track segments.

$$r_{TS} = \frac{|u - u_{tar}|}{u_{tar}} \quad (15)$$

- **Heading Alignment Reward:** Similarly leveraging the preview mechanism, we designate the heading at the look-ahead point on the racing line as the target heading  $\varphi_{tar}$ . This reward incentivizes precise vehicle pose control.

$$r_H = \frac{1}{1 + (\varphi - \varphi_{tar})^2} \quad (16)$$

### 3.3. Dynamics Constraints

The vehicle's stability region within the sideslip angle-yaw rate  $\beta - \omega$  phase plane is characterized by incorporating explicit priors on vehicle dynamics control, thereby constructing an explicit safe operating envelope as illustrated

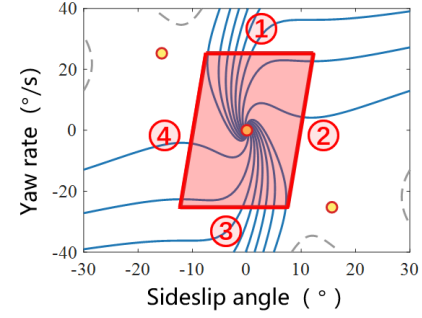


**Figure 7:** Illustration of the vehicle stability envelope based on the  $\beta - \omega$  phase plane.

in Fig. 7. This approach strictly confines the agent's policy updates within the dynamically feasible region, ensuring handling stability while the vehicle pursues limit performance.

As derived in [25], boundaries ① and ③ in Fig. 7 define the yaw rate limits with no longitudinal sliding:

$$|\omega_{ss,lim}| = \frac{\mu mg}{mu} = \frac{\mu g}{u} \quad (17)$$

Furthermore, the sideslip angle limits, boundaries ② and ④, are defined as:

$$\beta_{lim} = |\alpha_{r,peak}| + \frac{l_r \omega}{u} \quad (18)$$

where  $\alpha_{r,peak}$  is derived based on the Pacejka tire model [26]. By introducing the approximate limit slip angle as the saturation condition for rear tire force, the rear slip angle corresponding to the maximum lateral force is obtained as:

$$\alpha_{r,peak} = \arctan\left(\frac{3\mu mg l_f}{C_{ar}(l_f + l_r)}\right) \quad (19)$$

Based on the aforementioned safe operating envelope for yaw rate and sideslip angle, and leveraging the forward recursive safety feasibility of CBF [27], we employ a linear  $\alpha$  as a class  $\mathcal{K}_\infty$  function to construct the following physical constraints in CBF form:

- **Yaw Rate Constraint:**

$$\dot{h}_\omega \geq -\alpha h_\omega, \quad h_\omega = \frac{\mu g}{u} - |\omega| \quad (20)$$

- **Sideslip Angle Constraint:**

$$\begin{aligned} \dot{h}_{\beta 1} &\geq -\alpha h_{\beta 1}, & h_{\beta 1} &= \beta_{\max} - \beta \\ \dot{h}_{\beta 2} &\geq -\alpha h_{\beta 2}, & h_{\beta 2} &= \beta - \beta_{\min} \end{aligned} \quad (21)$$

where  $\beta_{\min}$  and  $\beta_{\max}$  correspond to the lower and upper bounds of the sideslip angle determined by boundaries ② and ④ in Fig. 7, respectively.

Accordingly, we define the instantaneous calculation formulas for the yaw rate cost  $c_\omega$  and the sideslip angle cost  $c_\beta$  as follows:

$$c_\omega = \max(-(\dot{h}_\omega + \alpha h_\omega), 0) \quad (22)$$

$$c_\beta = \max(-\min(\dot{h}_{\beta 1} + \alpha h_{\beta 1}, \dot{h}_{\beta 2} + \alpha h_{\beta 2}), 0) \quad (23)$$

Notably, this paper introduces a sliding window mechanism in the actual policy iteration process. This mechanism approximates the degree of violation by calculating the average cost within a time window, which is then used for subsequent parameter updates. Compared to directly using instantaneous values, this strategy effectively mitigates the impact of data noise and fluctuations from single time steps on training stability.

To maximize task rewards while strictly satisfying the aforementioned safety constraints, the RL problem is formulated as the following constrained optimization problem:

$$\begin{aligned} \max_{\theta} \quad & J_R(\pi_\theta) = \mathbb{E}_{\tau \sim \pi_\theta} \left[ \sum_{t=0}^T \gamma^t r_t + v \mathcal{H}(\pi_\theta(\cdot | s_t)) \right] \\ \text{s.t.} \quad & \mathbb{E}_{\tau \sim \pi_\theta} [c_\omega(s, a)] \leq d_\omega \\ & \mathbb{E}_{\tau \sim \pi_\theta} [c_\beta(s, a)] \leq d_\beta \end{aligned} \quad (24)$$

where  $\pi_\theta$  denotes the parameterized policy network, and  $J_R(\pi_\theta)$  represents the soft cumulative reward objective incorporating the entropy regularization term  $\mathcal{H}$ .  $d_\omega$  and  $d_\beta$  are the allowable cost thresholds.

Adaptive Lagrangian multipliers  $\lambda_\omega \geq 0$  and  $\lambda_\beta \geq 0$  are introduced to solve this problem, thereby transforming the constrained formulation into the following unconstrained optimization problem:

$$\begin{aligned} \min_{\lambda_\omega, \lambda_\beta \geq 0} \quad & \max_{\theta} L(\theta, \lambda_\omega, \lambda_\beta) \\ = \quad & J_R(\pi_\theta) - \sum_{k \in \{\omega, \beta\}} \lambda_k \left( \mathbb{E}_{(s,a) \sim \rho_{\pi_\theta}} [c_k(s, a)] - d_k \right) \end{aligned} \quad (25)$$

We adopt a primal-dual optimization method, performing alternating updates on the policy parameters  $\theta$  and the Lagrangian multipliers  $\lambda$ : With the policy parameters  $\theta$  fixed, the Lagrangian multipliers  $\lambda$  are updated via gradient ascent to increase the penalty weights for constraint-violating behaviors; With the Lagrangian multipliers  $\lambda$  fixed, the policy parameters  $\theta$  are updated to maximize the aforementioned objective. In this process, the maximization of task rewards is subject to the regularization constraints imposed by the weighted constraint costs.

### 3.4. Two-Stage Curriculum Design and RL Agent Training

To balance convergence efficiency in the early stages of training with the maximization of performance potential in the later stages, this paper proposes a two-stage training strategy. This strategy partitions the entire training process into two distinct stages: "Trajectory Guidance" and "High-Speed Exploration," utilizing a preset training step threshold,  $T_{switch}$ , as the criterion for stage transition. This design enables the agent to graduate from trajectory imitation to the autonomous exploration of the vehicle's dynamic boundaries.

- **Expert Trajectory Guidance Stage:** The target speed within the target speed tracking reward function,  $r_{TS}$ , is designated as the reference speed at the corresponding point on the MCRL. This leverages the prior knowledge embedded in the MCRL to facilitate the agent's rapid mastery of fundamental racing maneuvers, such as heavy braking before corner entry and path maintenance at the apex.
- **High-Speed Exploration Stage:** The target speed is reset to the maximum physically allowable speed of the racing vehicle. The removal of the MCRL speed constraints aims to overcome the conservatism inherent in the prior trajectory. It incentivizes the agent to explore within a broader state space, thereby uncovering faster lap times that surpass the MCRL baseline.

We employ Cost Critic networks,  $Q_C$ , for the accurate evaluation of potential constraint violation risks by estimating the expected cumulative constraint costs. For the  $k$ -th constraint, where  $k \in \{\omega, \beta\}$ , the parameters  $\xi_k$  of the Cost Critic are updated by minimizing the following Mean Squared Error (MSE) loss function,  $\mathcal{L}_{Cost}$ :

$$\mathcal{L}_{Cost}(\xi_k) = \mathbb{E}_{(s,a,c_k,s') \sim \mathcal{D}} \left[ \left( Q_{C_k}^{\xi_k}(s, a) - y_{c_k} \right)^2 \right] \quad (26)$$

where the target value  $y_{c_k}$  is defined as:

$$y_{c_k} = c_k + \gamma(1-d) \max_{j=1,2} Q_{C_k, target}^{\xi_j}(s', a') \quad (27)$$

The optimization objective of the Actor network is to maximize the reward while satisfying safety constraints. We integrate the constraint terms into the objective function and introduce a ReLU-based truncation mechanism, applying penalties only when the predicted cost exceeds the preset threshold  $d_k$ . This design creates a "safety dead-zone," allowing the agent to focus on task performance within the safe region and avoiding unnecessary conservative behavior. The loss function  $\mathcal{L}_{Actor}$  for the actor is defined as:

$$\begin{aligned} \mathcal{L}_{Actor}(\theta) = \mathbb{E}_{s \sim \mathcal{D}, a \sim \pi_\theta} \quad & \underbrace{\left[ \alpha \log \pi_\theta(a | s) - \min_{i=1,2} Q_{\psi_i}(s, a) \right]}_{\text{Reward Objective}} \\ & + \underbrace{\sum_{k \in \{\omega, \beta\}} \lambda_k \cdot \text{ReLU} \left( \max_{j=1,2} Q_{C_k}^{\xi_j}(s, a) - d_k \right)}_{\text{Violation Penalty}} \end{aligned} \quad (28)$$

where  $\psi$  denotes the parameters of the critic network.

The Lagrangian multipliers  $\lambda_k$  are updated via Dual Ascent. The corresponding loss function  $\mathcal{L}_{Lag}$ , which aims to maximize the dual objective, is given by:

$$\mathcal{L}_{Lag}(\lambda_k) = -\lambda_k (\bar{C}_k - d_k) \quad (29)$$

where  $\bar{C}_k$  is the average predicted cost of the current batch.

Specifically, the pseudocode for TraD-RL is presented in Algorithm 1.

**Algorithm 1** TraD-RL Algorithm

**Input:** Max training steps  $T_{max}$ , start training threshold  $T_{start}$ , stage switch threshold  $T_{switch}$ , safety cost thresholds  $d_\omega, d_\beta$ , batch size  $N$ .

**Initialize:** Randomly initialize Actor network  $\pi_\theta$ , Critic networks  $Q_{\psi_{1,2}}$ , safety Cost-Critic networks  $Q_{\xi_{1,2}}^\omega, Q_{\xi_{1,2}}^\beta$ ; initialize Lagrangian multipliers  $\lambda_\omega, \lambda_\beta$ ; initialize target network parameters  $\psi', \xi'$ ; initialize experience replay buffer  $\mathcal{D}$  and cost replay buffer  $\mathcal{D}_{cost}$ .

- 1: Solve for MCRL according to Eq. (13) based on the track map.
- 2: **for** current step  $t = 1 \rightarrow T_{max}$  **do**
- 3:   Obtain environmental observation  $o_t$  including augmented observation  $o_{MCRL}$ .
- 4:   Select action  $a_t \sim \pi_\theta(o_t)$  according to the current policy.
- 5:   Execute current action  $a_t$ , obtain basic rewards, obtain racing line related rewards according to Eqs. (14) to (16), and calculate costs according to Eqs. (22) and (23).
- 6:   Store tuple  $\langle o_t, a_t, r_t, o_{t+1} \rangle$  in  $\mathcal{D}$ ; store tuple  $\langle c_{\omega,t}, c_{\beta,t} \rangle$  in  $\mathcal{D}_{cost}$ .
- 7:   **if**  $t > T_{start}$  **then**
- 8:     Randomly sample  $N$  tuples from  $\mathcal{D}$  and  $\mathcal{D}_{cost}$ :  
 $\{ \langle o_i, a_i, r_i, o_{i+1} \rangle \}_{i=1 \dots N}$  and  $\{ \langle c_{\omega,i}, c_{\beta,i} \rangle \}_{i=1 \dots N}$ .
- 9:     Update Cost-Critic and Value networks using Eq. (26).
- 10:     Update Policy network using Eq. (28).
- 11:     Update Lagrangian multipliers using Eq. (29).
- 12:     Update entropy regularization parameter  $v$ .
- 13:     Soft update target networks and target cost networks:  
 $\psi'_1 \leftarrow \epsilon \psi_1 + (1 - \epsilon) \psi'_1, \quad \psi'_2 \leftarrow \epsilon \psi_2 + (1 - \epsilon) \psi'_2$   
 $\xi'_1 \leftarrow \epsilon \xi_1 + (1 - \epsilon) \xi'_1, \quad \xi'_2 \leftarrow \epsilon \xi_2 + (1 - \epsilon) \xi'_2$
- 14:   **end if**
- 15: **end for**

## 4. Experiment Studies

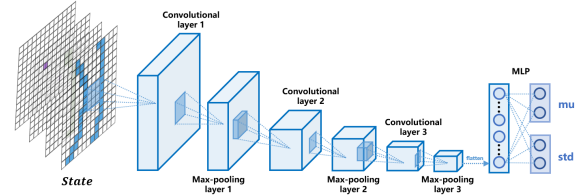
### 4.1. Experiment Setup

**Environment Setup** The simulation environment is based on the Berlin Tempelhof Airport Street Circuit, a renowned venue for the FIA Formula E Championship, as illustrated in Fig. 8. Spanning 2.469 km with 17 turns [28], the track is characterized by its compact and twisty geometric features, which impose stringent demands on the autonomous racing vehicle's handling rhythm and instant decision-making capabilities.

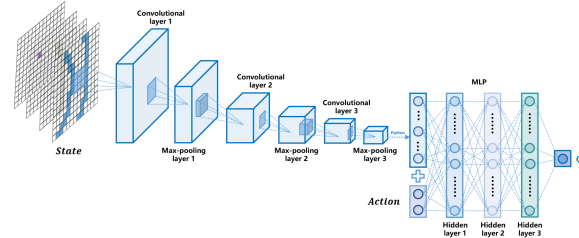
**Algorithm Setup** The Actor network, shown in Fig. 9a, utilizes a convolutional neural network (CNN) backbone to extract features from the occupancy grid observation, followed by a Multi-Layer Perceptron (MLP) to output the mean and standard deviation of the action distribution. The critic and cost critic networks, shown in Fig. 9b, adopt a similar CNN structure for state processing. The extracted feature vectors are then concatenated with the action vector



**Figure 8:** Aerial view of the Berlin Tempelhof Airport Street Circuit (Formula E Berlin E-Prix).



(a) The Actor network architecture for action distribution output.



(b) The Critic (and Cost-Critic) network architecture for value estimation.

**Figure 9:** Schematic diagram of the proposed network architectures.

and fed into an MLP to estimate the Q-value of the state-action pair.

The detailed experimental parameters are as follows:

- **Training Scale:** The total number of training steps is set to  $T_{max} = 250,000$ . The agent begins the learning process after an initial exploration phase of  $T_{start} = 20,000$  steps. The two-stage training step threshold,  $T_{switch} = 200,000$ . For performance evaluation, the number of test episodes is  $K = 20$ .
- **Buffer Capacity:** The capacity for both the replay buffer  $\mathcal{D}$  and the cost replay buffer  $\mathcal{D}_{cost}$  is set to 200,000.
- **Network Structure:** The CNN backbone utilizes hidden channels of [32, 64, 128]. The subsequent Multi-Layer Perceptron (MLP) consists of hidden units with a configuration of [256, 256, 256].
- **Optimization:** The learning rate for both the Actor and Critic networks is  $1 \times 10^{-4}$ , while the learning rate for the adaptive Lagrangian multipliers is set to  $5 \times 10^{-5}$ . The discount factor for future rewards and costs is  $\gamma = 0.99$ .

**Table 1**  
Vehicle dynamics parameters used in the experiment.

Parameter	Symbol	Value	Unit
Mass	$m$	800	kg
Length	$L$	4.7	m
Width	$w_{veh}$	2	m
CG to Front Axle	$l_f$	2.115	m
CG to Rear Axle	$l_r$	1.88	m
Front Cornering Stiffness	$C_{af}$	64,000	N/rad
Rear Cornering Stiffness	$C_{ar}$	64,000	N/rad

**Vehicle Setup** The vehicle dynamics parameters used in the experiment are summarized in Table 1.

## 4.2. Comparison Models

- **Proximal Policy Optimization (PPO):** A robust on-policy algorithm that utilizes clipping for policy updates to ensure training stability.
- **Deep Deterministic Policy Gradient (DDPG):** A classic off-policy algorithm based on the deterministic policy gradient theorem.
- **Trajectory-Aided Learning (TAL)[29]:** A DRL framework that incorporates the optimal trajectory into the learning formulation to guide agents for high-speed racing.
- **Ours (TraD-RL):** The proposed MCRL-guided and dynamics-constrained reinforcement learning algorithm.

## 4.3. Evaluating Metrics

To evaluate the racing performance and safety level of the autonomous racing agents, the following performance metrics are employed:

### 4.3.1. Racing Performance Metrics

- **Lap Average Speed:** The average speed of the racing vehicle during a single lap. As a fundamental evaluation metric, it directly reflects the absolute racing capability of the agent on the track.
- **Lap Time:** The time required for the racing vehicle to complete a single lap. By comprehensively considering both the driving speed and trajectory length, this metric effectively reflects the agent's global speed planning level and trajectory optimization capability.

### 4.3.2. Safety Metrics

- **Time-averaged Lap  $\omega$ -unsafe Times:** The number of times the vehicle violates the yaw rate dynamic boundaries (i.e., boundaries ① and ③ in Fig. 7) within a single lap. To eliminate evaluation bias caused by varying lap completion times across different algorithms, this metric is normalized using the lap time.
- **Time-averaged Lap  $\beta$ -unsafe Times:** The number of times the vehicle violates the center-of-mass sideslip angle dynamic boundaries (i.e., boundaries ② and ④ in Fig. 7) within a single lap. Similarly normalized by the lap time, this metric, together with the yaw rate violation

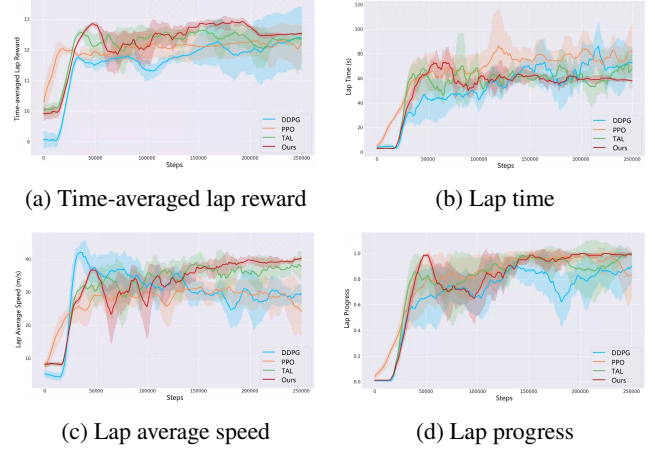


**Figure 10:** Learning curves of multi-dimensional performance metrics for different algorithms during the training process: (a) Time-averaged lap reward; (b) Lap time; (c) Lap average speed; (d) Lap progress.

times, constitutes a core indicator for evaluating the vehicle's dynamic stability at handling limits.

- **Lap Progress:** The percentage of the track completed before the vehicle collides or runs off the track; if the lap is successfully completed, the progress reaches 100%. This metric is utilized to macroscopically measure the overall safety and stability of the driving policy.

## 4.4. Comparison Results and Analysis

### 4.4.1. Training Results

Fig. 10a illustrates the time-averaged lap reward (i.e., the ratio of the total cumulative lap reward to the completion time) of each algorithm during the training process, showing that all four algorithms successfully reach a stable convergence state in the later stages of training. Meanwhile, Fig. 10b and Fig. 10c present the learning curves for lap time and lap average speed, respectively. As core metrics for evaluating the racing performance of autonomous vehicles, these two indicators intuitively reflect the agent's global speed planning level and comprehensive racing performance on complex tracks. Benefiting from the prior guidance of MCRL, the proposed method (Ours) stably achieves a lower lap time and a higher average lap speed after convergence compared to the other baseline algorithms, which thoroughly demonstrates that the incorporation of MCRL effectively breaks through the vehicle's racing bottlenecks. Furthermore, Fig. 10d demonstrates the lap progress during training, a critical indicator for evaluating policy safety. Due to the complete absence of safety constraint mechanisms, the lap progress of the DDPG algorithm exhibits severe fluctuations and remains generally low; the policy clipping mechanism of PPO implicitly enhances training stability to a certain extent, resulting in slightly better completion performance than DDPG. Guided globally by the racing line, the TAL method effectively prevents the vehicle from deviating from the normal driving trajectory. However, due to the lack of explicit vehicle dynamics constraints, it still struggles to

**Table 2**

Quantitative comparison of racing performance and safety metrics across different algorithms during the testing process.

Algorithm	Racing Performance		Safety	
	Lap Average Speed (m/s)	Lap Time (s)	Time-averaged lap $\omega$ -unsafe Times	Time-averaged lap $\beta$ -unsafe Times
DDPG	30.49	75.65	18.31	8.34
PPO	28.37	84.67	14.53	1.86
TAL	38.67	61.31	17.65	5.85
Ours	39.79	58.83	16.50	4.61

avoid safety violations under limit-handling conditions, such as high-speed cornering. In contrast, by synergistically integrating the MCRL global guidance and CBF-based explicit dynamics constraints, the proposed method stably ensures a 100% lap progress after approximately 15k training steps, demonstrating remarkable safety guarantees and training stability in high-speed racing scenarios.

#### 4.4.2. Testing Results

The racing performance metrics in Table 4.1 demonstrate the superiority of the proposed method (Ours), which significantly outperforms DDPG, PPO, and TAL in both lap average speed and lap time. Specifically, our method achieves an improvement in lap average speed of 30.50%, 40.25%, and 2.90% over DDPG, PPO, and TAL, respectively, corresponding to reductions in lap time of 22.23%, 30.52%, and 4.05%. These significant gains indicate that the MCRL introduced in our framework provides critical path references and velocity guidance for motion planning. Consequently, the agent is able to fully exploit the track width and road friction limits to maintain higher speeds through tight corners, effectively pushing the vehicle's performance toward the theoretical limits of time-optimal control.

Regarding the safety metrics presented in Table 4.1, although high-speed racing inherently increases control difficulty, the proposed method demonstrates superior safety performance. Compared to DDPG and TAL, our method reduces the time-averaged lap  $\omega$ -unsafe times by 9.89% and 6.52%, respectively, and substantially decreases the time-averaged lap  $\beta$ -unsafe times by 44.72% and 21.20%, respectively. The significant reduction in sideslip angle violations directly highlights the algorithm's advantage in lateral stability control. This improvement indicates that the explicit dynamics constraints effectively suppress excessive lateral drift during limit cornering and significantly mitigate heading oscillations caused by control overshoot. Such precise regulation of lateral dynamics prevents "spin-outs," which are frequently encountered at high speeds. It is worth noting that the yaw rate constraint in Eq. (20) explicitly involves longitudinal speed. While strict enforcement typically forces a vehicle to decelerate, our method achieves the highest average lap speed with minimal violations. This suggests that our explicit dynamics constraints do not simply trade speed for safety; instead, they guide the vehicle to operate

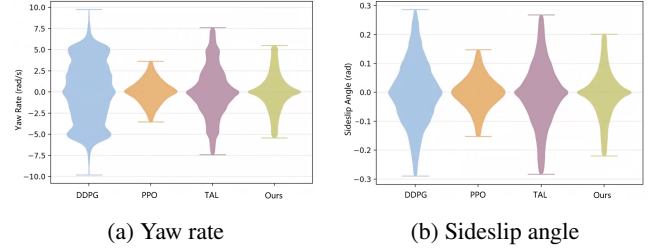


**Figure 11:** Statistical distribution of vehicle dynamics states for different algorithms during testing: (a) Yaw rate; (b) Sideslip angle.

efficiently along the boundaries of the safe envelope. In contrast, while the PPO algorithm achieves the lowest violation counts, this is entirely attributed to its overly conservative driving policy that sacrifices racing performance to avoid instability. However, such a strategy does not align with the practical requirements of high-speed racing.

Fig. 11 further illustrates the probability density distributions of the vehicle's yaw rate and center-of-mass sideslip angle during the testing phase. It is evident that, after incorporating explicit dynamics constraints, the data distribution of the proposed method exhibits greater convergence compared to DDPG and TAL. The values are predominantly concentrated within the stable region near zero, accompanied by a significant reduction in the long-tail distributions associated with instability. This provides compelling evidence that the CBF-based dynamics constraints effectively confine the vehicle states within a safe feasible set, substantially suppressing severe oscillations and sideslip instability during high-speed driving, and ultimately achieving a dual optimization of performance and safety.

#### 4.4.3. Case Study

Fig. 12 (left) visualizes the trajectory and speed distributions of the two methods in a continuous corner. It can be observed that the TAL method (green trajectory) exhibits evident trajectory jitter and abrupt curvature variations during the corner entry and exit phases, with the trajectory presenting zigzag deflections. In contrast, under the global guidance of MCRL, the trajectory planned by the proposed method features extremely smooth curvature transitions. Such smooth geometric characteristics enable the autonomous racing vehicle to execute more coherent

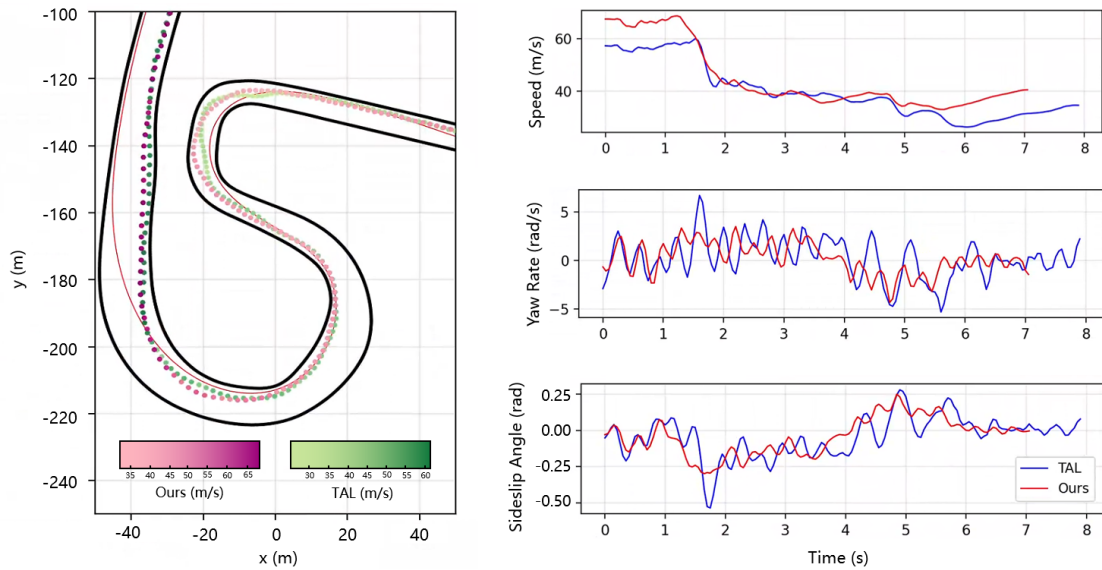


**Figure 12:** Experimental results comparison in a continuous corner (S-curve) section of the Berlin Tempelhof Airport Street Circuit. Left: Trajectory and speed heat map distributions of TAL and the proposed method (Ours), with the red solid line representing the MCRL. Right: Time-series comparison of vehicle speed, yaw rate, and sideslip angle during the cornering process.

speed control commands, demonstrating a more robust driving style. According to the speed profile (Fig. 12, top-right), the proposed method reaches a high initial speed of nearly 70 m/s before corner entry. Benefiting from the superior racing line guidance, it executes reasonable early braking for a smooth entry. During the mid-corner and exit phases, the generated trajectory maintains a better radius of curvature with smooth transitions. This geometric advantage eliminates the need for abrupt braking corrections, enabling the vehicle to stably sustain a minimum speed of approximately 30 m/s. This smooth racing line, which prevents excessive speed degradation, accumulates a massive momentum advantage for straight-line acceleration after exiting the corner, ultimately achieving superior overall cornering efficiency.

Furthermore, high-speed continuous cornering is a critical limit-handling scenario highly susceptible to vehicle lateral slip and instability. As shown in Fig. 12 (middle-right and bottom-right), the TAL method generates remarkably high peak values of 7.05 rad/s and 0.64 rad for these two metrics, respectively. These peaks are accompanied by high-frequency oscillations, indicating that the vehicle repeatedly approaches or enters physical instability. This unstable state is the exact physical root cause of the zigzag deflections observed in the green trajectory. Conversely, the proposed method utilizes explicit dynamics constraints to strictly limit the peak yaw rate and sideslip angle to 3.76 rad/s and 0.38 rad. This precise regulation effectively suppresses abnormal state peaks and mitigates dynamic oscillations. Consequently, it yields the smooth, high-quality driving trajectory depicted in Fig. 12 (left). The comprehensive comparison of trajectory performance and dynamic states thoroughly validates that the proposed method can effectively guarantee the handling stability and safety of the racing vehicle under limit conditions while pursuing extreme racing performance.

#### 4.5. Ablation Experiment

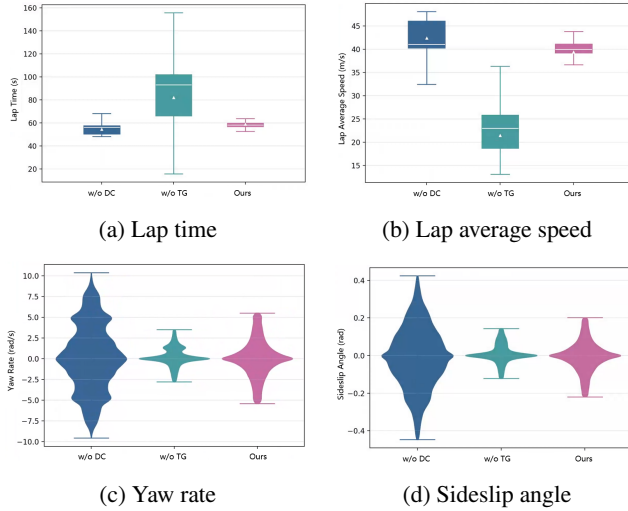
To further validate the effectiveness of the core modules in the proposed TraD-RL algorithm, we conducted ablation studies in the testing environment. Specifically, two ablated variants are implemented by removing the trajectory guidance module (denoted as w/o TG) and the explicit dynamics constraints module (denoted as w/o DC). Fig. 13(a) and (b), and Table 3 collectively present the racing performance metrics of the different ablation algorithms. Comparing the proposed method (Ours) with removing the trajectory guidance method (w/o TG), it is evident that the inclusion of the trajectory guidance module significantly elevates the vehicle's racing limits. Specifically, the introduction of this module leads to a 23.38% reduction in lap time and an 83.44% increase in average lap speed. This indicates that without global trajectory guidance, the agent is highly susceptible to falling into an overly conservative local optimum to satisfy safety requirements. Specifically, the agent drastically reduces speed in exchange for safety, as demonstrated by the extremely low average lap speed (21.47 m/s) of w/o TG in Table 3. The incorporation of MCRL successfully breaks this deadlock, providing rational speed and path references for the vehicle under limit-handling conditions.

Regarding safety performance metrics, Table 3 reveals substantial differences among the algorithms. A comparison between our method and removing the dynamics constraints method (w/o DC) shows that the addition of the dynamics constraints module substantially reduces the time-averaged lap  $\omega$ -unsafe times and time-averaged lap  $\beta$ -unsafe times by 10.28% and 39.90%, respectively. Although the w/o DC method demonstrates comparable top-speed performance to our method, this is achieved entirely at the severe expense of driving safety. Furthermore, observing the distribution characteristics of the box plots in Fig. 13(a) and (b), the

**Table 3**

Quantitative comparison of racing performance and safety metrics across different ablation algorithms during the testing process.

Algorithm	Racing Performance		Safety	
	Lap Average Speed (m/s)	Lap Time (s)	Time-averaged lap $\omega$ -unsafe Times	Time-averaged lap $\beta$ -unsafe Times
w/o DC	41.40	55.59	18.39	7.67
w/o TG	21.47	82.15	9.95	4.10
Ours	39.39	58.83	16.50	4.61

**Figure 13:** Performance and safety comparison of different ablation algorithms during the testing phase: (a) Box plot of lap time; (b) Box plot of average lap speed; (c) Statistical distribution of yaw rate; (d) Statistical distribution of sideslip angle.

proposed method exhibits the most compact distribution for both lap time and lap speed. This implies that the dynamics constraints module not only guarantees absolute safety for individual laps but also greatly enhances the robustness and control stability of the policy across multiple trials.

Finally, by analyzing the violin plots of the vehicle dynamics states in Fig. 13(c) and (d), the underlying physical mechanisms of the dynamics constraints module can be understood more intuitively. Due to the absence of explicit safety boundaries, the yaw rate and sideslip angle distributions for the w/o DC method are extremely wide, featuring prominent long-tail distributions caused by severe vehicle sideslip and tail-flicking. Conversely, after incorporating the CBF-based dynamics constraints, the proposed method strictly truncates and confines the vehicle's dynamic states within the safe envelope, resulting in a significantly more concentrated data distribution. This result provides compelling evidence for the decisive role of dynamics constraints in preventing extremely hazardous behaviors, such as out-of-control spin-outs, and further confirms that underlying dynamic stability is the prerequisite for achieving an extremely fast and safe driving policy.

Consequently, the results of the ablation study demonstrate that each component in TraD-RL is crucial, which fully validates the effectiveness of integrating trajectory guidance and dynamics constraints.

## 5. Conclusion

This paper proposes a Trajectory guidance and Dynamics constraints Reinforcement Learning (TraD-RL) decision-making and control framework for autonomous racing. The methodology integrates expert prior knowledge through several key components: the MCRL is utilized to provide global path and velocity guidance, which effectively narrows the exploration space and enhances learning efficiency. Simultaneously, explicit vehicle dynamics constraints are enforced based on CBF to characterize the safe operating envelope, ensuring handling stability by suppressing excessive yaw rate and sideslip angle. Furthermore, a two-stage curriculum learning strategy is implemented to facilitate a smooth transition from stable trajectory following to high-speed limit exploration. The experiment environment is based on the Berlin Tempelhof Airport Street Circuit. Simulation results show that TraD-RL significantly enhances both lap speed and driving stability on complex tracks, maintaining the vehicle's dynamic state within a safe operating envelope even under limit-handling conditions. The ablation studies further confirm that the trajectory guidance module is essential for elevating racing limits and breaking conservative local optima, while the explicit dynamics constraints serve as a fundamental prerequisite for suppressing physical instability and ensuring policy robustness across multiple trials. Overall, TraD-RL provides a viable solution for achieving a synergistic optimization of performance and safety in high-speed autonomous racing scenarios.

## CRedit authorship contribution statement

**Bo Leng:** Conceptualization, Funding acquisition, Formal analysis, Project administration, Writing - review & editing. **Weiqi Zhang:** Conceptualization, Data curation, Formal analysis, Investigation, Methodology, Software, Supervision, Validation, Visualization, Writing - original draft, Writing - review & editing. **Zhuoren Li:** Conceptualization, Formal analysis, Methodology, Project administration, Supervision, Writing - original draft, Writing - review & editing. **Lu Xiong:** Funding acquisition, Formal analysis, Resources, Supervision. **Guizhe Jin:** Methodology, Resources,

Software, Supervision. **Ran Yu:** Methodology, Resources, Software, Visualization. **Chen Lv:** Conceptualization, Supervision, Writing - review & editing.

## Data availability

The data and materials used to support the findings of this study are available from the corresponding author upon reasonable request.

## Declaration of competing interest

The authors declare that they have no known competing financial interests or personal relationships that could have appeared to influence the work reported in this paper.

## Acknowledgments

This work is supported by the National Natural Science Foundation of China under Grant No.52522219, and No.52325212.

## References

- [1] A. Muraleedharan, I. Simões, G. Pau, Randomized model predictive control for autonomous racing, in: 2025 IEEE Intelligent Vehicles Symposium (IV), IEEE, 2025, pp. 1078–1085.
- [2] D. Kalaria, C. Maheshwari, S. Sastry,  $\{\alpha\}$ -racer: Real-time algorithm for game-theoretic motion planning and control in autonomous racing using near-potential function, arXiv preprint arXiv:2412.08855 (2024).
- [3] A. Langmann, L. Ögretmen, F. Werner, J. Betz, Online velocity profile generation and tracking for sampling-based local planning algorithms in autonomous racing environments, arXiv preprint arXiv:2505.05157 (2025).
- [4] J. Betz, T. Betz, F. Fent, M. Geisslinger, A. Heilmeyer, L. Hermansdorfer, T. Herrmann, S. Huch, P. Karle, M. Lienkamp, et al., Tum autonomous motorsport: An autonomous racing software for the indy autonomous challenge, *Journal of Field Robotics* 40 (4) (2023) 783–809.
- [5] A. Wischnewski, M. Geisslinger, J. Betz, T. Betz, F. Fent, A. Heilmeyer, L. Hermansdorfer, T. Herrmann, S. Huch, P. Karle, et al., Indy autonomous challenge-autonomous race cars at the handling limits, in: 12th International Munich Chassis Symposium 2021: chassis. tech plus, Springer, 2022, pp. 163–182.
- [6] A2RL - Abu Dhabi Autonomous Racing League, Autonomous car race, <https://a2rl.io/autonomous-car-race>, accessed: 2024-05-20 (2024).
- [7] Z. Demeter, M. Hell, G. Hajgató, Lessons learned from an autonomous race car competition, *Engineering Proceedings* 79 (1) (2024) 25.
- [8] B. Leng, R. Yu, C. Tu, L. Xiong, A. Eichberger, Z. Li, Seamless overtaking maneuvers for automated driving: Integrated motion planning based on hybrid model predictive control, *IEEE Transactions on Industrial Electronics* (2026).
- [9] J. F. Bongard, V. L. Krieger, B. Lohmann, Dynamic constraint tightening for nonlinear mpc for autonomous racing via contraction analysis, in: 2025 IEEE Intelligent Vehicles Symposium (IV), IEEE, 2025, pp. 2288–2295.
- [10] M. Brown, J. C. Gerdes, Coordinating tire forces to avoid obstacles using nonlinear model predictive control, *IEEE Transactions on Intelligent Vehicles* 5 (1) (2019) 21–31.
- [11] J. Betz, H. Zheng, A. Liniger, U. Rosolia, P. Karle, M. Behl, V. Krovi, R. Mangharam, Autonomous vehicles on the edge: A survey on autonomous vehicle racing, *IEEE Open Journal of Intelligent Transportation Systems* 3 (2022) 458–488.
- [12] Y. Song, H. Lin, E. Kaufmann, P. Dürr, D. Scaramuzza, Autonomous overtaking in gran turismo sport using curriculum reinforcement learning, in: 2021 IEEE international conference on robotics and automation (ICRA), IEEE, 2021, pp. 9403–9409.
- [13] E. Kaufmann, L. Bauersfeld, A. Loquercio, M. Müller, V. Koltun, D. Scaramuzza, Champion-level drone racing using deep reinforcement learning, *Nature* 620 (7976) (2023) 982–987.
- [14] J. Kabzan, L. Hewing, A. Liniger, M. N. Zeilinger, Learning-based model predictive control for autonomous racing, *IEEE Robotics and Automation Letters* 4 (4) (2019) 3363–3370.
- [15] H. Xue, E. L. Zhu, J. M. Dolan, F. Borrelli, Learning model predictive control with error dynamics regression for autonomous racing, in: 2024 IEEE International Conference on Robotics and Automation (ICRA), IEEE, 2024, pp. 13250–13256.
- [16] C. Weaver, C. Tang, C. Hao, K. Kawamoto, M. Tomizuka, W. Zhan, Betail: Behavior transformer adversarial imitation learning from human racing gameplay, *IEEE Robotics and Automation Letters* 9 (8) (2024) 7302–7309.
- [17] B. D. Evans, H. W. Jordaan, H. A. Engelbrecht, Safe reinforcement learning for high-speed autonomous racing, *Cognitive Robotics* 3 (2023) 107–126.
- [18] Z. Li, B. Leng, L. Xiong, A. Eichberger, C. Huang, J. Hu, Safety-enhanced deep reinforcement learning for autonomous driving: Dare to make mistakes to learn better and faster, *IEEE Transactions on Intelligent Transportation Systems* (2026).
- [19] F. Fuchs, Y. Song, E. Kaufmann, D. Scaramuzza, P. Dürr, Super-human performance in gran turismo sport using deep reinforcement learning, *IEEE Robotics and Automation Letters* 6 (3) (2021) 4257–4264.
- [20] P. R. Wurman, S. Barrett, K. Kawamoto, J. MacGlashan, K. Subramanian, T. J. Walsh, R. Capobianco, A. Devlic, F. Eckert, F. Fuchs, et al., Outracing champion gran turismo drivers with deep reinforcement learning, *Nature* 602 (7896) (2022) 223–228.
- [21] C. Tang, B. Abbatematteo, J. Hu, R. Chandra, R. Martín-Martín, P. Stone, Deep reinforcement learning for robotics: A survey of real-world successes, *Annual Review of Control, Robotics, and Autonomous Systems* 8 (1) (2025) 153–188.
- [22] P. Ladosz, L. Weng, M. Kim, H. Oh, Exploration in deep reinforcement learning: A survey, *Information Fusion* 85 (2022) 1–22.
- [23] Z. Zhang, Q. Liu, Y. Li, K. Lin, L. Li, Safe reinforcement learning in autonomous driving with epistemic uncertainty estimation, *IEEE Transactions on Intelligent Transportation Systems* 25 (10) (2024) 13653–13666.
- [24] A. Heilmeyer, A. Wischnewski, L. Hermansdorfer, J. Betz, M. Lienkamp, B. Lohmann, Minimum curvature trajectory planning and control for an autonomous race car, *Vehicle System Dynamics* (2020).
- [25] Z. Zhu, X. Tang, Y. Qin, Y. Huang, E. Hashemi, A survey of lateral stability criterion and control application for autonomous vehicles, *IEEE Transactions on Intelligent Transportation Systems* 24 (10) (2023) 10382–10399.
- [26] J.-H. Ryu, D. Ogay, S. Bulavintsev, H. Kim, J.-S. Park, Development and experiences of an autonomous vehicle for high-speed navigation and obstacle avoidance, in: *Frontiers of Intelligent Autonomous Systems*, Springer, 2013, pp. 105–116.
- [27] A. D. Ames, S. Coogan, M. Egerstedt, G. Notomista, K. Sreenath, P. Tabuada, Control barrier functions: Theory and applications, in: 2019 18th European control conference (ECC), Ieee, 2019, pp. 3420–3431.
- [28] FIA Formula E, Berlin circuit, [fiaformulae.com](http://www.fiaformulae.com), archived from the original on July 13, 2015. Accessed: 2015-07-13 (2015). URL <http://www.fiaformulae.com/en/calendar/berlin-eprix/berlin-circuit.aspx>
- [29] B. D. Evans, H. A. Engelbrecht, H. W. Jordaan, High-speed autonomous racing using trajectory-aided deep reinforcement learning, *IEEE Robotics and Automation Letters* 8 (9) (2023) 5353–5359.



**Bo Leng** received the Ph.D. degree in vehicle engineering from Tongji University, Shanghai, China. He is currently an Associate Professor with the School of Automotive Studies, Tongji University. His current research interests include the dynamic control of distributed drive electric vehicles and motion planning and control of intelligent vehicles. He has won the First Prize in the China Automobile Industry Technology Invention Award and the First Prize in the Shanghai Science and Technology Progress Awards in 2020 and 2022. He has been selected into the Young Elite Scientists Sponsorship Program of the China Association for Science and Technology in 2022.



**Ran Yu** received his B.E. degree in vehicle engineering from the School of Automotive Engineering, Harbin Institute of Technology, Weihai, China, in 2024. He is currently pursuing his M.E. degree in vehicle engineering from the College of Automotive and Energy Engineering, Tongji University, Shanghai, China. His research interests include safe reinforcement learning, and motion planning and control of intelligent vehicles.



**Weiqi Zhang** received his B.E. degree in vehicle engineering from Tongji University, Shanghai, China, in 2025. Currently, he is working toward the Ph.D. degree at the Institute of Intelligent Vehicles, Tongji University, Shanghai, China. His research interests include autonomous, racing, safe reinforcement learning, and end-to-end autonomous driving.



**Chen Lv** received the joint Ph.D. degree from the Department of Automotive Engineering, Tsinghua University, China, and the EECS Department, University of California, Berkeley, USA, in January 2016. He is an Associate Professor with the School of Mechanical and Aerospace Engineering, Nanyang Technological University (NTU), Singapore. He also holds joint appointments as the Research Director of NTU, Vice President Research Office, the Director of M.Sc. degree in robotics and intelligent systems, a Thrust Lead in AI with the Continental-NTU Corporation Laboratory, and the Cluster Director in Future Mobility Solutions with ERI@N. He was as a Research Fellow with the Advanced Vehicle Engineering Center, ranfield University, U.K., from 2016 to 2018. He joined NTU, as a Nanyang Assistant Professor and has founded the Automated Driving and Human-Machine System (AutoMan) Research Laboratory in June 2018. His research focuses on advanced vehicle control and intelligence, where he has contributed four books, over 200 papers, and received 12 granted patents and five patent applications.



**Zhuoren Li** received his Ph.D. degree in vehicle engineering in 2025 and his B.E. degree in engineering mechanics in 2019, Tongji University, Shanghai, China. His current research interests include safe reinforcement learning, large language model enhanced end-to-end autonomous driving, interaction decision-making, and motion planning of autonomous vehicles.



**Lu Xiong** received the Ph.D. degree in vehicle engineering from Tongji University, Shanghai, China, in 2005. He is currently the Vice President and a Professor with the School of Automotive Studies, Tongji University. His current research interests include the dynamic control of distributed drive electric vehicles, motion planning and control of intelligent vehicles, and all-terrain vehicles. He won the First Prize in the Shanghai Science and Technology Progress Awards in 2013, 2020, and 2022. He was a recipient of the National Science Fund for Distinguished Young Scholars.



**Guizhe Jin** received the bachelor's degree in mechanical engineering from Harbin Institute of Technology, Weihai, China, in 2019. He is currently pursuing the master's degree with the College of Automotive and Energy Engineering, Tongji University, Shanghai, China. His research interests mainly focus on motion planning for autonomous vehicles via deep reinforcement learning.